NANO LETTERS

Open Access
This article is licensed under CC-BY 4.0

pubs.acs.org/NanoLett
Letter

Ultranarrow Line Width Room-Temperature Single-Photon Source from Perovskite Quantum Dot Embedded in Optical Microcavity

Tristan Farrow,*,‖ Amit R. Dhawan,‖ Ashley R. Marshall, Alexander Ghorbal, Wonmin Son, Henry J. Snaith, Jason M. Smith, and Robert A. Taylor

Cite This: *Nano Lett.* 2023, 23, 10667−10673

Read Online
ACCESS | Metrics & More | Article Recommendations

ABSTRACT: Ultranarrow bandwidth single-photon sources operating at room-temperature are of vital importance for viable optical quantum technologies at scale, including quantum key distribution, cloud-based quantum information processing networks, and quantum metrology. Here we show a room-temperature ultranarrow bandwidth single-photon source generating single-mode photons at a rate of 5 MHz based on an inorganic $CsPbI_3$ perovskite quantum dot embedded in a tunable open-access optical microcavity. When coupled to an optical cavity mode, the quantum dot room-temperature emission becomes single-mode, and the spectrum narrows down to just ∼1 nm. The low numerical aperture of the optical cavities enables efficient collection of high-purity single-mode single-photon emission at room-temperature, offering promising performance for photonic and quantum technology applications. We measure 94% pure single-photon emission in a single-mode under pulsed and continuous-wave (CW) excitation.

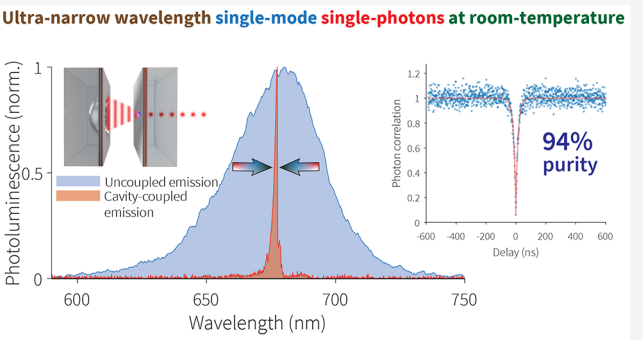

KEYWORDS: *single-photon source, lead-halide perovskite nanocrystals, all-inorganic perovskites, optical microcavity, ultranarrow line width photons, quantum technologies*

Ultranarrow line width room-temperature (RT) single-photons are essential for photonic quantum technologies[1,2] but their fabrication poses a challenge. Probabilistic single-photon sources such as attenuated lasers are nonideal,[3] while high-performance single-photon emission has only been demonstrated at cryogenic temperatures.[4,5] However, cryogenic cooling is expensive and cumbersome, so it hinders practical use. Peltier coolers are cryogen-free and offer a cheaper alternative to cryogenic cooling; however, room-temperature operation sets the gold-standard for viable ultranarrow band single-photon sources. While room-temperature single-photon sources such as colloidal quantum dots suffer from multiexciton emission[6,7] and nitrogren vacancy centers show significant phonon sideband emission,[8,9] perovskite quantum dots (PQDs) are promising emitters for cost-effective, scalable, spectrally pure, and color-tunable single-photon sources for quantum technology applications.[10,11] Quantum confinement in PQDs maintains the nonclassical character of the optical signal at RT,[12] but like their semiconductor counterparts at higher temperatures, their emission line width widens by up to tens of nanometers due to phonon broadening, which undermines their technological potential. Possible strategies have been proposed for producing narrow line widths (35−65 meV) at room-temperature through targeted chemical treatment of the dot surface to quench low-energy surface phonon modes responsible for broadening.[13] However, restoring the line widths to almost cryogenic-environment-like line widths at RT is a significantly more demanding task, which may be achieved by constructing a single-photon source comprising an emitter embedded in a tunable optical microcavity.[14] This configuration offers the advantages of narrowband emission, excellent emission directionality and high single-mode photon collection at RT. Where light−matter engineering systems such as plasmonic antennas[15,6,16,17] demonstrate very high Purcell factor due to ultralow mode volume, open-access optical microcavity systems as demonstrated here offer narrowband single-mode emission and wavelength tunability. Additionally, PQDs can be dispersed in a large range of nonpolar solvents after synthesis, so can be spin-coated on a wide variety of surfaces for integration within devices.

Received: June 1, 2023
Revised: November 20, 2023
Accepted: November 21, 2023
Published: November 28, 2023

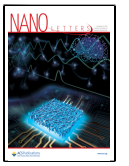

Downloaded via 90.199.148.63 on March 13, 2024 at 07:08:32 (UTC).
See https://pubs.acs.org/sharingguidelines for options on how to legitimately share published articles.

ACS Publications
© 2023 The Authors. Published by American Chemical Society

https://doi.org/10.1021/acs.nanolett.3c02058
Nano Lett. 2023, 23, 10667−10673

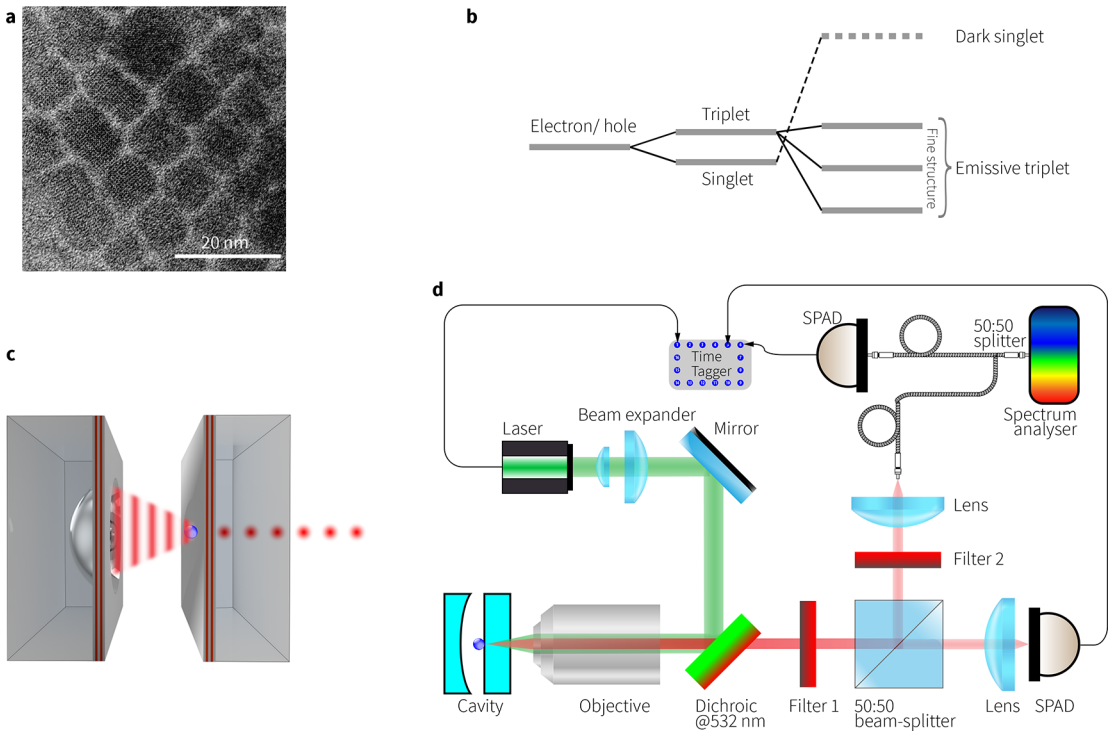

Figure 1. (a) Transmission electron image of a superlattice of $CsPbI_3$ showing individual PQDs and their size. (b) Energy level diagram illustrating the exciton fine structure typical of $CsPbX_3$ PQDs with an emissive triplet and a dark singlet on an inverted energy ladder resulting from the interplay between strong spin−orbit coupling and symmetry breaking. (c) Illustration of PQD−microcavity coupling. The open-access optical microcavity is formed by a planar mirror (supporting the emitter) and a concave mirror. Wavelength tuning is achieved by changing the distance separating the mirrors. (d) Layout of the optical setup used for cavity coupling and characterization. Filter 1 is a 665 ± 75 nm bandpass filter to allow PL emission to the SPADs (single photon avalanche photodiode), and Filter 2 is a 650 ± 100 nm bandpass filter to prevent optical crosstalk.

We demonstrate such a single-photon source in air at RT featuring an inorganic $CsPbI_3$ PQD (Figure 1a) coupled to an optical microcavity (Figure 1c). We observe that the narrowband TEM_{00} mode emission from individual PQDs embedded in the microcavity exhibits strong photon antibunching under both continuous-wave (CW) and pulsed excitation with single-photon purity of 94% in a single-mode with ∼1 nm line width. In this way we produce bright, pure-color emission with a detected photon rate of 5×10^6 per second. We also note the challenges associated with PQDs due to photoinduced degradation or photobleaching in intense light fields. Advances in passivation strategies relying on targeted nanocrystal surface chemistry approaches, including surface treatments, passivating ligands, core/shell structures, and solid-state ligand exchange, result in fewer defects and will improve PQD robustness and device fabrication yields.[18]

PQD emitters offer excellent optical properties, including fast polarized emission with long coherence times and high quantum yields (95%).[19] Their short-lifetime photoluminescence (PL) and high quantum yield at cryogenic temperatures offers excellent performance for an unprocessed chemically synthesized nanocrystal system.[20−23] The emission wavelength of PQDs can be tuned over a wide range (430−730 nm) by modifying their chemical composition, and they maintain optical performance and narrow line widths up to RT.[13] This, coupled to the low-cost and ease of synthesis, brings them tantalizingly close to industrial scaling-up since most applications operate in air at ambient temperatures.

The custom-fabricated open Fabry−Pérot microcavities used in this study offer a unique combination of small mode volumes (<1 μ m^3) and Q-factors of up to (>10^4),[24] combined with full in situ wavelength tunability of the cavity mode. They consist of a planar mirror, onto which the PQDs are deposited by spin-coating from solution, and a curved mirror, where the distance and angle between the mirrors is controlled using piezoelectric nanopositioning stages. The mirror coatings are tailored to the design wavelength of the PQDs. The operation wavelengths of the cavities can range from 450 to 950 nm and higher depending on the choice of mirror-coating.

Photoluminescence from PQD film was characterized using the experimental setup of Figure 1d) prior to coupling into the optical microcavity. Figure 2a,b compare the PL peaks of single out-of-cavity PQDs at 4 K in vacuum and at RT in air. At cryogenic temperatures, their characteristic PL spectrum can be fitted with a Lorentzian profile with line width 0.6 nm (1.7 meV), which is within the typical range of 0.6−2 meV[25] at cryogenic temperatures for single $CsPbI_3$ nanocrystals with edge length of ∼15 nm. At RT, the out-of-cavity fwhm is more than an order of magnitude wider at ∼40 nm, which is attributed to homogeneous broadening due to low-energy phonon-coupling[13,26] present on the surface of the quantum dots.

Our time-resolved photoluminescence (TRPL) measurements on PQDs (Figure 2d,e) show a typical lifetime of 0.4 ns at 4 K and 12.2 ns at RT, respectively, consistent with observed behavior[27,28] and attributed to the fission of excitons into free carriers at higher temperatures.[29] The state lifetime at cryogenic temperature is comparable to the 180−300 ps lifetimes[30,19] reported in lead halide PQDs. We calculated the decay lifetime using a monoexponential fit of the TRPL curve typical of the transition rate dynamics in two-level systems like PQDs excited at low powers.[19,25] We note that the fast

https://doi.org/10.1021/acs.nanolett.3c02058
Nano Lett. 2023, 23, 10667−10673

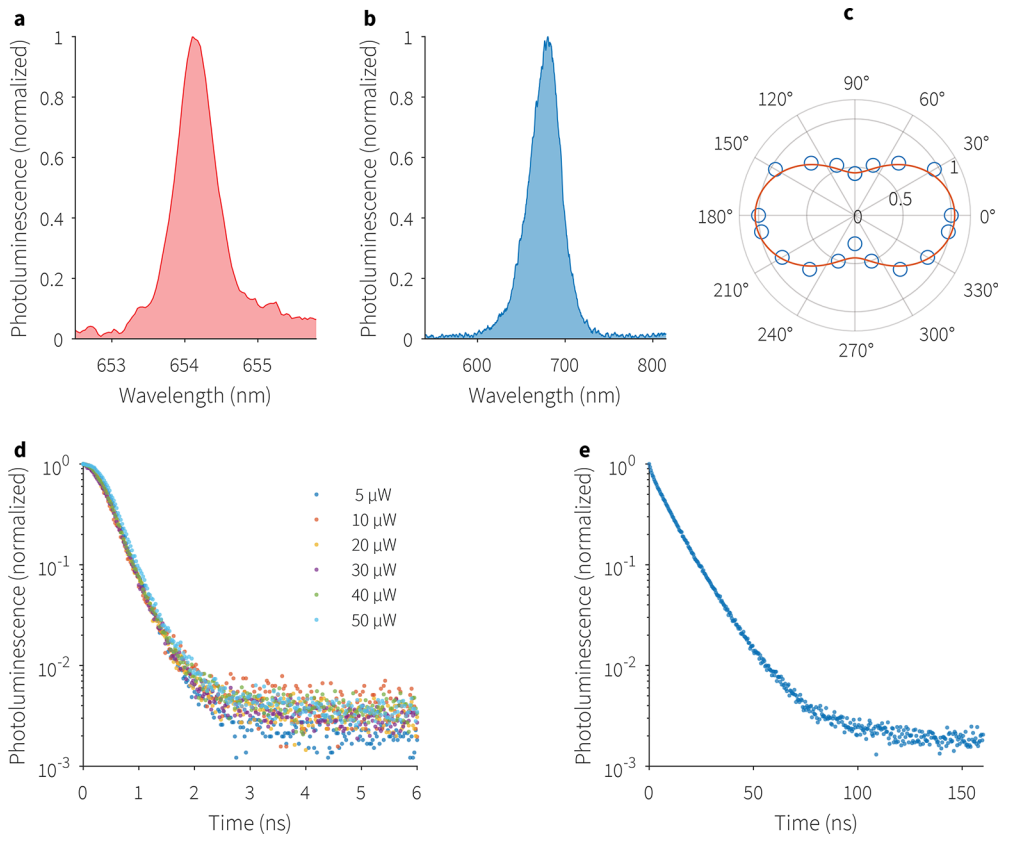

Figure 2. (a) Out-of-cavity photoluminescence spectrum of a PQD at 4 K showing a fwhm of 0.6 nm. (b) RT emission spectrum of a PQD, which shows a fwhm of ~40 nm. Polarization measurement at 10 K shows a 40% degree of linear polarization in (c). Out-of-cavity TRPL measurements on a PQD, (d) at different powers at 4 K and (e) at RT under 0.3 μW, showing lifetimes of 0.4 ns (typical) and 12.2 ns, respectively.

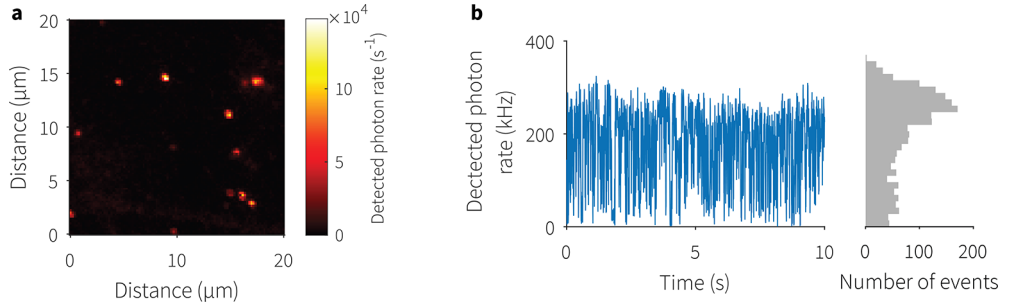

Figure 3. (a) Out-of-cavity confocal laser scan of a region on the planar mirror spin-coated with PQDs. Well-separated single PQDs are selected for cavity coupling. (b) Typical photoluminescence blinking of a PQD from the used batch; the histogram bin width is 5 ms. The PQD was under 532 nm CW excitation.

component of the time-resolved PL signal (Figure 2d,e) is more than 2.5 orders of magnitude more intense than the long-lived residual tail of the emission, attributed to delayed carrier recombination during thermalization and trapping.[31] Detector dark counts account for the flat nonzero intensity segment of the delayed tail of the emission.

The noteworthy optical performance can in part be attributed to the presence of fast, optically active, triplet states (Figure 1b), present uniquely in lead halide perovskites.[32,25,33] Spin-forbidden triplet transitions delay PL emission, but in these systems, they become dipole-allowed due to unusually strong spin−orbit coupling from heavy Pb ions. This results in bright triplet states (the only known example of a material with this property) which can help explain the bright PL intensity observed in PQDs. A Rashba-type effect due to symmetry perturbation inverts the energies of singlet and triplet exciton states and lifts the fine structure degeneracy to reveal the ultranarrow line widths within the fine structure in the orthorhombic and tetragonal phases of the crystal,[32,25] but not in the orthogonal phase where the splitting is degenerate. Different PQDs exhibit different decay times, where the variations in lifetime can be attributed to differences in the sizes of the nanocrystals, hence different quantum confinement energies.[34]

POLARIZED PHOTONS

Polarization measurements at cryogenic temperatures highlight that the PQD emits partially polarized light. Plotting the fluorescence intensity $I(\theta)$ as a function of a linear polarizer angle θ (Figure 2c) reveals that PQD emission is polarized,

https://doi.org/10.1021/acs.nanolett.3c02058
Nano Lett. 2023, 23, 10667−10673

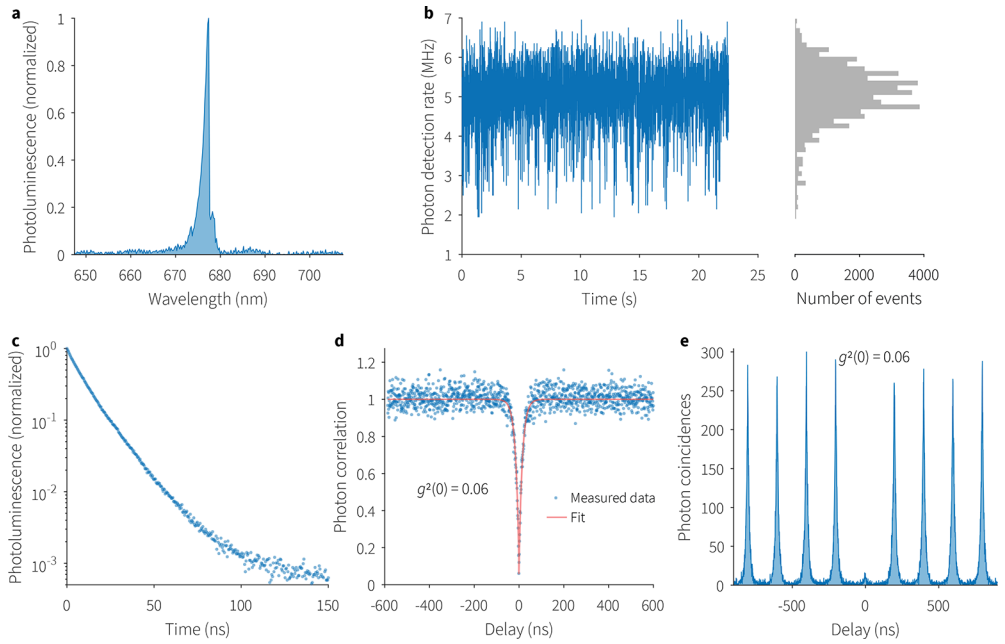

Figure 4. (a) RT emission from a PQD coupled to a TEM_{00} mode of the optical cavity centered at 677 nm and with a fwhm of 1.1 nm, decayed monoexponentially with a lifetime of 12.7 ns (c) and emitted single TEM_{00} mode single-photons with a purity of 94% as shown by continuous (d) and pulsed (e) HBT measurements. (b) Detected photon rate of 5 MHz (histogram bin width of 5 ms) under CW pumping.

which is consistent with other reports.[30] Measured data is fitted to Malus' law, $I(\theta) = I_{min} + (I_{max} - I_{min}) \cos^2 \theta$, where $I(\theta)$ is the intensity at polarizer angle θ, and I_{max} and I_{min} are the maximum and minimum intensities, respectively. The degree of linear polarization, defined as $(I_{max} - I_{min})/(I_{max} + I_{min})$, is found to be 40%. Polarization of photons in single-photon sources with >50% efficiency and near unity indistinguishability can be achieved with polarized cavities.[35] Single-photon devices that emit polarized light are advantageous in technological applications such as entanglement-based quantum key distribution.

COUPLING A PQD TO A MICROCAVITY

The planar mirror with spin-coated $CsPbI_3$ PQDs was scanned confocally (Figure 3a), and individual PQDs, which inherently emit single-photons, were selected for cavity coupling and driven toward the mirror with concave features using nanopositioning motion controllers to create an optical microcavity. This precavity coupling characterization was carried out with the emitter facing the objective to facilitate light extraction. Most PQDs from the tested batch blinked or fluoresced intermittently under 532 nm laser excitation, as shown in Figure 3b. The photobleaching of individual PQDs, which is well-known,[12] especially in an intense light field such as inside a cavity at RT, can make closing the cavity and recording measurements challenging. The PQDs remain optically active for periods lasting seconds to minutes when the cavity closes due to the increased field intensity and photodegradation, aggravated by pulsed illumination, after which time the emission becomes too weak for in-cavity measurements. Due to photodegradation of single PQDs, from 100 PQDs, approximately 10 of them could successfully be coupled to the cavity for measurements.

The PQD in the cavity was excited by shining a laser through the planar mirror, and the cavity was finely tuned to couple maximum fluorescence from the PQD to the optical cavity TEM_{00} mode. This design featuring a half-symmetric open-access resonator configuration offers two advantages: First, any emitter on the planar mirror can be coupled to a wavelength tunable optical cavity, and second, the concave mirror facilitates optimal coupling by reducing light dissipation due to scattering. Moreover, milling multiple concave features with different radii of curvature on the same plinth permit different coupling possibilities. The cavity-emitted light was collected from the planar mirror side using a 0.85 numerical aperture coverslip-corrected objective. The low angle of cavity emission allows efficient collection even with lower numerical aperture objectives or lenses.[36]

The finesse $\mathcal{F}$ of our optical-cavity was recorded to be 100, which yields a quality factor, $Q = q\mathcal{F} = 3 \times 100 = 300$. Here, q is the axial mode index of the optical cavity. Increasing q increases the quality factor and the effective mode volume V (0.5 μm^3 in our case) and hinders electromagnetic field confinement in low-width cavities as used here.[24,8] The curved mirror was 4.4 μm wide with a 8 μm radius of curvature. The Purcell factor $F_P = \xi^2 \frac{3\lambda_c^3}{4\pi^2} \frac{Q}{V}$, where λ_c is the wavelength of the main cavity mode and ξ is the dipole orientation factor that accounts for the coupling between the emitter and the cavity field. $\xi^2 = 1$ for a perfectly aligned dipole, and $\xi^2 = 1/3$ if all possible dipole orientations are averaged. Assuming randomly oriented PQD dipoles, this gives $F_P = 4.7$ and can reach a maximum value of 14 for a perfectly aligned dipole. This moderate value of F_P is attributed to the relatively low Q value of our cavity, which can be increased by using higher finesse cavities.

SINGLE-MODE EMISSION

The PL spectrum of a single PQD at RT is significantly broader compared to that at cryogenic temperatures. When the PQD is inserted into the microcavity, its emission is forced

https://doi.org/10.1021/acs.nanolett.3c02058
Nano Lett. 2023, 23, 10667−10673

into the optical modes of the cavity, which acts as a narrow bandpass filter.

By changing the cavity length using piezo-electric actuators to adjust the cavity modes, PQD emission was coupled into a cavity mode, which makes the emission narrowband and single-mode. Figure 2a displays the emission from a TEM_{00} with an axial mode index of 3. Compared with the 40 nm wide RT free-space emission of a PQD in Figure 2b, its cavity-coupled emission results in a single-mode with a fwhm of 1 nm. The open-access microcavity design permits straightforward modification of the axial and the lateral emitter position that enables wavelength tunability and coupling of the emitter to different cavity modes. This design has been employed to demonstrate wavelength tunable narrowband RT emission line widths from other single-emitters as well.[8,36] The coupling of a PQD to a cavity mode leads to a modification of the density of the optical states. This Purcell effect alters the spontaneous decay process of the PQD such that its emission is forced into the narrow cavity mode, to which it is coupled.

SINGLE-PHOTON EMISSION

We performed photon correlation measurements in a Hanbury Brown and Twiss (HBT) setup (Figure1d) on the emission from a PQD coupled to an optical cavity TEM_{00} mode (Figure 4a) using CW (Figure 4c) and pulsed (Figure 4d) lasers. The single-photon emission efficiency is recorded by noting the probability of photon detection when the delay between the single photon detection events at both the detectors (SPADs) is zero. This is depicted as the zero-delay peak in the histograms of Figure 4d,e.

Pulsed excitation poses additional challenges for systems prone to photobleaching due to the high energy in individual pulses. In both regimes, we recorded a 94% single-photon purity. Remarkably, the detected photon rate was 5 MHz; Figure 4b shows the actual photon rate measured by the photon-detector without taking into account any optical system and photodectection losses. Figure 4c shows the time-decay of the PL emission from a single in-cavity PQD in air at RT with a monoexponential lifetime of 12.7 ns.

We have demonstrated a single-photon source in air at RT based on inorganic $CsPbI_3$ perovskite PQDs embedded in a microcavity with a single-photon purity of 94% in CW and pulsed mode operation at a rate of 5 MHz. Critically, coupling the emission into the cavity mode reduced the emission line width to just ∼1 nm without the need for cryogenic cooling. The reproducible synthesis of PDQs and ease of deposition directly onto cavity surfaces result in a highly reproducible low-cost single-photon system with the potential for transformational impact on quantum technologies at scale with the advent of robust PQDs.

An ultraviolet fused silica slip (Spectrosil 2000) was diced to create flat-topped plinth of height 100 μm and top area of 300 μm × 300 μm on which smooth spherical concave features are created using focused ion-beam milling. Here, we used a concave feature of depth 0.3 μm and radius of curvature of 8 μm. A planar substrate made of the same material is used for the planar mirror as well. By depositing alternate layers of SiO_2 and Ta_2O_5 by ion-beam sputtering, the dielectric Bragg mirror reflectors are created. The 97.5 ± 0.5% and >99.9% reflectivity of the planar and plinth mirrors at a central wavelength of 690 nm (selected due to the PQD emission wavelength), respectively, allow the creation of an optimum optical microcavity where light is extracted from the planar mirror.

CHEMICAL SYNTHESIS

Reagents: All chemicals were purchased from Sigma-Aldrich and used without further purification. Lead iodide (PbI_2, 99%), cesium carbonate Cs_2CO_3, Reagent Plus 99%), 1-octadecene (ODE, technical grade, 90%), oleic acid (OA, technical grade, 90%), oleylamine (OLAm, technical grade, 70%), methyl acetate (MeAc, anhydrous, 99.5%), octane (anhydrous, 99%) toluene (anhydrous, 99.8%), and ethylenediaminetetraacetic acid (EDTA, ACS Reagent, 99.4%).

Perovskite quantum dots (PQDs) were synthesized following the hot injection method adapted from the literature.[37] Each step up until the PQDs purification was done using standard Schlenk line techniques to keep the reaction air-free under nitrogen. First, 0.407 g of Cs_2CO_3, 1.25 mL of OA, and 20 mL of ODE were added to a 100 mL 3-necked flask and degassed for 1 h under vacuum (flask 1). Flask 1 was then heated to 150 °C, and the vacuum was switched to an over pressure of nitrogen when the flask temperature was 100 °C. Flask 1 was left stirring at 150 °C until all of the solid Cs_2CO_3 was dissolved, indicating that the Cs-oleate had formed. Flask 1 was then cooled to 130 °C before being used in the next step.

Into a 250 mL 3-necked round-bottomed flask, 0.5 g of PbI_2 and 25 mL of the ODE were degassed and then heated to 120 °C under vacuum (flask 2). Meanwhile, 2.5 mL of OA and 2.5 mL of OLAm were heated on a hot plate set at 130 °C. The hot OA-OLAm mixture was injected into flask 2 and left under vacuum until all the PbI_2 had dissolved. Flask 2 was switched from vacuum to nitrogen and the temperature control unit was set to 180 °C. Immediately upon reaching 180 °C, 2 mL of the Cs-oleate solution from flask 1 was injected into flask 2. Flask 1 was then moved from the heating mantle to an ice bath as quickly as possible after injection. Once flask 2 had cooled, the reaction was removed from the Schlenk line and exposed to ambient conditions for the purification steps.

The reaction mixture from flask 2 was separated into 2 centrifuge tubes (10 mL in each), and 70 mL of MeAc was used to precipitate the PQDs. The PQDs were then centrifuged to form a pellet, and the supernatant was discarded. The pellets were redispersed in 5 mL of hexane, then precipitated with 7 mL of methyl acetate, and centrifuged again. This pellet was dispersed in 2 mL of octane and stored in a glass vial in the fridge. Some precipitate collected on the bottom of the vial overnight; this is avoided when removing the sample from the vial.

For the RT measurements, the $CsPbI_3$ QDs were treated with EDTA by stirring 1 mL of PQDs with 5 mg of EDTA overnight to improve photostability and filtered through a 200 nm mesh. Size-selective centrifugation was used in order to obtain monodispersed PQDs. The original PQD solution in octane was diluted by at least 10-fold and then centrifuged at low speeds (2000−3000 rpm) for 30 min. The resulting supernatant was used for measurements, while the small pellet that formed was discarded. A well-dissolved (in toluene) and concentration-calibrated PMMA solution was prepared and added to the sample which was then spin-coated onto the flat DBR mirror. This resulted in a monodispersed deposition of PQDs at the right concentration (1−5 PQDs/10 μm^2 with a target of 1 PQD/10 μm^2, corresponding to the cavity diameter). Coupling of single-PQDs poses a challenge if the sample is prone to the clustering of PQDs, even after calibrating the colloidal concentration to the cavity diameter

https://doi.org/10.1021/acs.nanolett.3c02058
Nano Lett. 2023, 23, 10667−10673

and laser footprint. Clusters couple to the cavity more readily, revealing its modal structure but are unsuitable for single-photon generation, which requires the coupling of single PQDs.

A poly(methyl methacrylate) (PMMA) coat helped to isolate the PQDs from air, albeit with marginal effect as compared to previous attempts where no PMMA was used, and attenuated the signal intensity by approximately 10−15%. The collection efficiency can be improved by centrifuging the PQDs, covering them in PMMA with thickness λ_c, and by replacing the final SiO_2 layer of the planar DBR, since the refractive indices of the two materials match. Chemical passivation such as with EDTA[38] offers an additional strategy for improving the durability of the PQDs against bleaching. We note that there are no restrictions on the operation-temperature of the cavities since they can work as well in the cryogenic regime as they do at RT.

For the 4 K measurements, solutions of $CsPbI_3$ nanocrystals in toluene were spin-coated at 4000 rpm for 30 s onto glass substrates. Various dilutions (in toluene) were tried until the concentration allowed for the resolution of the emission spectrum from individual PQDs.

The optical properties of the PQDs at RT were characterized using a confocal micro-photoluminescence setup. The PQDs were excited with a 532 nm Oxiuss diode-pumped solid-state CW laser and a 532 nm PicoQuant PDL800-D pulsed laser at a repetition rate of 5 MHz with a pulse width of 50 ps. The two microcavity mirrors were mounted on Thorlabs Nanomax 300 piezo-electric stages to control the cavity configuration. Both the laser pump beam excitation and cavity fluorescence collection were through the planar mirror side using a coverslip corrected 0.85 numerical aperture Olympus LCPLFLN100XLCD objective. For the out-of-cavity measurements, the same setup was used but without the curved mirror, and the emitter, placed on the planar mirror, faced the objective. Single-photon detection and counting were performed using Exelitas SPCM-AQRH-14 SPADs and Swabian Instruments Time Tagger 20. Cryogenic temperature measurements were carried out in a Janis ST-500 continuous flow liquid helium cryostat. The excitation was performed with a 532 PicoQuant PDL800-D pulsed laser, and the emission was collected with a Mitutoyo 0.8 NA objective lens using a confocal setup.

AUTHOR INFORMATION

Corresponding Author

Tristan Farrow − *Department of Physics, University of Oxford, Oxford OX1 3PU, United Kingdom;* orcid.org/0000-0002-2393-9745; Email: tristan.farrow@physics.ox.ac.uk

Authors

Amit R. Dhawan − *Department of Materials, University of Oxford, Oxford OX1 3PH, United Kingdom*

Ashley R. Marshall − *Department of Physics, University of Oxford, Oxford OX1 3PU, United Kingdom*

Alexander Ghorbal − *Department of Physics, University of Oxford, Oxford OX1 3PU, United Kingdom*

Wonmin Son − *Sogang University, Mapo-gu, Seoul 04107, South Korea*

Henry J. Snaith − *Department of Physics, University of Oxford, Oxford OX1 3PU, United Kingdom;* orcid.org/0000-0001-8511-790X

Jason M. Smith − *Department of Materials, University of Oxford, Oxford OX1 3PH, United Kingdom*

Robert A. Taylor − *Department of Physics, University of Oxford, Oxford OX1 3PU, United Kingdom;* orcid.org/0000-0003-2578-9645

Complete contact information is available at: https://pubs.acs.org/10.1021/acs.nanolett.3c02058

Author Contributions

[‖]T.F. and A.R.D. contributed equally to this work.

Notes

The authors declare no competing financial interest.

ACKNOWLEDGMENTS

The authors acknowledge support from the Gordon and Betty Moore Foundation, EPSRC grant EP/V028642/1, and the National Research Foundation of Korea grants NRF-2020M3E4A1080070 and NRF-2020M3H3A1107840. W.S. acknowledges the Korea Institute For Advanced Study.

REFERENCES

(1) O'Brien, J. L.; Furusawa, A.; Vučković, J. Photonic quantum technologies. *Nat. Photonics* **2009**, *3*, 687−695.

(2) Wang, J.; Sciarrino, F.; Laing, A.; Thompson, M. G. Integrated photonic quantum technologies. *Nat. Photonics* **2020**, *14*, 273−284.

(3) Eisaman, M. D.; Fan, J.; Migdall, A.; Polyakov, S. V. Invited review article: Single-photon sources and detectors. *Rev. Sci. Instrum.* **2011**, *82*, 071101.

(4) Senellart, P.; Solomon, G.; White, A. High-performance semiconductor quantum-dot single-photon sources. *Nat. Nanotechnol.* **2017**, *12*, 1026.

(5) Wang, Y.; et al. Deterministic photon source interfaced with a programmable silicon-nitride integrated circuit. *npj Quantum Information* **2023**, *9*, 94.

(6) Dhawan, A. R.; et al. Extreme multiexciton emission from deterministically assembled single-emitter subwavelength plasmonic patch antennas. *Light: Science & Applications* **2020**, *9*, 33.

(7) Morozov, S.; et al. Purifying single photon emission from giant shell cdse/cds quantum dots at room temperature. *Nanoscale* **2023**, *15*, 1645−1651.

(8) Dolan, P. R.; et al. Robust, tunable, and high purity triggered single photon source at room temperature using a nitrogen-vacancy defect in diamond in an open microcavity. *Opt. Express* **2018**, *26*, 7056−7065.

(9) Senichev, A.; Martin, Z. O.; Peana, S.; Sychev, D.; Xu, X.; Lagutchev, A. S.; Boltasseva, A.; Shalaev, V. M. Room-temperature single-photon emitters in silicon nitride. *Sci. Adv.* **2021**, *7*, No. eabj0627.

(10) Hu, F.; et al. Superior optical properties of perovskite nanocrystals as single photon emitters. *ACS Nano* **2015**, *9*, 12410−12416.

(11) Yang, Z.; Pelton, M.; Bodnarchuk, M. I.; Kovalenko, M. V.; Waks, E. Spontaneous emission enhancement of colloidal perovskite nanocrystals by a photonic crystal cavity. *Appl. Phys. Lett.* **2017**, *111*, 221104.

(12) Park, Y.-S.; Guo, S.; Makarov, N. S.; Klimov, V. I. Room temperature single-photon emission from individual perovskite quantum dots. *ACS Nano* **2015**, *9*, 10386−10393.

(13) Rainò, G.; et al. Ultra-narrow room-temperature emission from single cspbbr3 perovskite quantum dots. *Nat. Commun.* **2022**, *13*, 1−8.

(14) Di, Z.; et al. Controlling the emission from semiconductor quantum dots using ultra-small tunable optical microcavities. *New J. Phys.* **2012**, *14*, No. 103048.

(15) Curto, A. G.; et al. Unidirectional emission of a quantum dot coupled to a nanoantenna. *Science* **2010**, *329*, 930−933.

(16) Hoang, T. B.; Akselrod, G. M.; Mikkelsen, M. H. Ultrafast room-temperature single photon emission from quantum dots coupled to plasmonic nanocavities. *Nano Lett.* **2016**, *16*, 270−275.
(17) Dhawan, A. R.; Nasilowski, M.; Wang, Z.; Dubertret, B.; Maître, A. Fabrication of efficient single-emitter plasmonic patch antennas by deterministic in situ optical lithography using spatially modulated light. *Adv. Mater.* **2022**, *34*, No. 2108120.
(18) VanOrman, Z. A.; Weiss, R.; Medina, M.; Nienhaus, L. Scratching the surface: Passivating perovskite nanocrystals for future device integration. *J. Phys. Chem. Lett.* **2022**, *13*, 982−990.
(19) Utzat, H.; et al. Coherent single-photon emission from colloidal lead halide perovskite quantum dots. *Science* **2019**, *363*, 1068−1072.
(20) Michler, P.; et al. A quantum dot single-photon turnstile device. *Science* **2000**, *290*, 2282−2285.
(21) Santori, C.; Pelton, M.; Solomon, G.; Dale, Y.; Yamamoto, Y. Triggered single photons from a quantum dot. *Phys. Rev. Lett.* **2001**, *86*, 1502−1505.
(22) Zwiller, V.; et al. Single quantum dots emit single photons at a time: Antibunching experiments. *Appl. Phys. Lett.* **2001**, *78*, 2476−2478.
(23) Yuan, Z.; et al. Electrically driven single-photon source. *Science* **2002**, *295*, 102−105.
(24) Dolan, P. R.; Hughes, G. M.; Grazioso, F.; Patton, B. R.; Smith, J. M. Femtoliter tunable optical cavity arrays. *Opt. Lett.* **2010**, *35*, 3556−3558.
(25) Becker, M. A.; et al. Bright triplet excitons in caesium lead halide perovskites. *Nature* **2018**, *553*, 189−193.
(26) Zhou, X.; Zhang, Z. Electron−phonon coupling in $CsPbBr_3$. *AIP Advances* **2020**, *10*, 125015.
(27) Han, Q.; Wu, W.; Liu, W.; Yang, Q.; Yang, Y. Temperature-dependent photoluminescence of $CsPbX_3$nanocrystal films. *J. Lumin.* **2018**, *198*, 350−356.
(28) Li, J.; et al. Temperature-dependent photoluminescence of inorganic perovskite nanocrystal films. *RSC Adv.* **2016**, *6*, 78311−78316.
(29) Diroll, B. T.; Nedelcu, G.; Kovalenko, M. V.; Schaller, R. D. High-temperature photoluminescence of $CsPbX_3$(X = Cl, Br, I) nanocrystals. *Adv. Funct. Mater.* **2017**, *27*, 1606750.
(30) Rainò, G.; et al. Single cesium lead halide perovskite nanocrystals at low temperature: Fast single-photon emission, reduced blinking, and exciton fine structure. *ACS Nano* **2016**, *10*, 2485−2490.
(31) Park, Y.; et al. Coarse and fine-tuning of lasing transverse electromagnetic modes in coupled all-inorganic perovskite quantum dots. *Nano Research* **2021**, *14*, 108−113.
(32) Ying, G.; et al. Resonantly pumped bright-triplet exciton lasing in cesium lead bromide perovskites. *ACS Photonics* **2021**, *8*, 2699−2704.
(33) Sercel, P. C.; et al. Exciton fine structure in perovskite nanocrystals. *Nano Lett.* **2019**, *19*, 4068−4077.
(34) Zhao, Q.; et al. Size-dependent lattice structure and confinement properties in $cspbi_3$ perovskite nanocrystals: Negative surface energy for stabilization. *ACS Energy Letters* **2020**, *5*, 238−247.
(35) Wang, H.; He, Y.-M.; Chung, T.-H.; Hu, H.; Yu, Y.; Chen, S.; Ding, X.; Chen, M.-C.; Qin, J.; Yang, X. Towards optimal single-photon sources from polarized microcavities. *Nat. Photonics* **2019**, *13*, 770.
(36) Vogl, T.; Lecamwasam, R.; Buchler, B. C.; Lu, Y.; Lam, P. K. Compact cavity-enhanced single-photon generation with hexagonal boron nitride. *ACS Photonics* **2019**, *6*, 1955−1962.
(37) Swarnkar, A.; et al. Quantum dot−induced phase stabilization of α-$CsPbI_3$ perovskite for high-efficiency photovoltaics. *ACS Energy Letters* **2016**, *354*, 92−95.
(38) Hassan, Y.; et al. Ligand-engineered bandgap stability in mixed-halide perovskite LEDs. *Nature* **2021**, *591*, 72−77.

Recommended by ACS

Excitonic Quantum Coherence in Light Emission from $CsPbBr_3$ Metal-Halide Perovskite Nanocrystals
Dallas Strandell, Patanjali Kambhampati, *et al.*
DECEMBER 19, 2023
NANO LETTERS
READ

Sub-Single-Exciton Optical Gain in Lead Halide Perovskite Quantum Dots Revealed by Exciton Polarization Spectroscopy
Yuan Liu, Kaifeng Wu, *et al.*
NOVEMBER 16, 2023
JOURNAL OF THE AMERICAN CHEMICAL SOCIETY
READ

Hot Excitons Cool in Metal Halide Perovskite Nanocrystals as Fast as CdSe Nanocrystals
Dallas P. Strandell, Patanjali Kambhampati, *et al.*
DECEMBER 18, 2023
ACS NANO
READ

Ultrafast Control of the Optical Transition in Type-II Colloidal Quantum Wells
Junhong Yu, Cuong Dang, *et al.*
APRIL 21, 2023
ACS PHOTONICS
READ

Get More Suggestions >

https://doi.org/10.1021/acs.nanolett.3c02058
Nano Lett. 2023, 23, 10667−10673